Eur. Phys. J. B **10**, 223–231 (1999)

**THE EUROPEAN PHYSICAL JOURNAL B**

EDP Sciences


# In situ resistivity and magnetoresistance studies of Co/Au(111) single layers and bilayers

J. Corno[1], M. Galtier[1], D. Renard[1], J.P. Renard[2,a], and F. Trigui[3]

[1] Institut d'Optique Théorique et Appliquée[b], Bâtiment 503, Université Paris-Sud, BP 147, 91403 Orsay Cedex, France
[2] Institut d'Électronique Fondamentale[c], Bâtiment 220, Université Paris-Sud, 91405 Orsay Cedex, France
[3] Faculté des Sciences de Sfax, BP 763, Route de Soukra, 3038 Sfax, Tunisia

Received 3 November 1998 and Received in final form 18 January 1999

**Abstract.** We report here on resistance and magnetoresistance (MR) studies of ultrathin Co/Au(111) single sandwiches and bilayers with perpendicular magnetization. Resistance of the films was measured *in situ* in ultrahigh vacuum, during depositions and as a function of a perpendicular applied magnetic field. A large MR variation with the thickness of Au coverage was observed and compared to calculations. The coercive field of the Co films shows a drastic variation with the Au coverage thickness, which reflects the theoretical anisotropy variation. It was measured as a function of temperature. For the first time, the effect of interlayer interaction on the resistivity of a Co bilayer during the growth of Co top layer, is evidenced and compared to calculations. Finally, hysteresis loops of strongly antiferromagnetically coupled bilayers are investigated.

**PACS.** 75.70.Cn Interfacial magnetic properties (multilayers, magnetic quantum wells, superlattices, magnetic heterostructures – 75.70.Pa Giant magnetoresistance

## 1 Introduction

The ultrathin films consisting of a few atomic layers (AL) of Co on Au(111) substrate have been extensively studied. Indeed, they are very attractive because they exhibit a large interface magnetic anisotropy (IMA) [1], leading to perpendicular magnetization for Co thickness $t$, below a critical value $t^*$. In addition, Co single layers and bilayers, sandwiched by Au, exhibit large magnetoresistance (MR) effects revealed in early experiments [2] and explained later [3,4] by the giant magnetoresistance (GMR) mechanism established for antiferromagnetic Fe/Cr multilayers [5,6]. The oscillating character of the exchange coupling between Co layers separated by a Au(111) spacer layer was observed lately by MR and polar magneto-optical Kerr effect (PMOKE) [7]. The interlayer exchange interaction is alternately ferromagnetic (FM) and antiferromagnetic (AFM) with a period $\Lambda = 4.5$ AL, in good agreement with the theoretical predictions [8].

The magnetic properties of Co ultrathin films are mainly governed by surface and interface effects. For instance, the Co/vacuum IMA favors in-plane magnetization, whereas the large Co/Au(111) IMA, of opposite sign, favors perpendicular magnetization and is strongly dependent on the sharpness of the Co/Au interface [9–12]. A powerful experimental tool for studying these surface and interface effects is to follow the physical phenomena during the deposition of noble metal overlayer converting the naked surface into an interface. This was already done by PMOKE in ultrahigh vacuum [10] for Co/Au(111), and with overlayers of different metals [11]. In addition to their influence on magnetic anisotropy, the surface and interface play an important role in transport properties since they are a source of scattering for the conduction electrons.

In the present work, we report on *in situ* studies of resistance during the growth of the different films. Magnetoresistance loops of Co/Au(111) layers and bilayers are performed, always *in situ*, after each deposition. After the introduction, Section 1, the experimental set up and process are shortly described in Section 2. In Section 3, the experimental data on Co/Au(111) single layers are compared to a simple model. Section 4 is devoted to Co/Au(111) bilayers; the effect of the Au overlayer thickness on resistance, MR and coercive field is investigated for FM and AFM interaction between the Co films and compared to phenomenological models. The summary and conclusion are given in Section 5.

## 2 Experimental set up, process and samples

The samples were grown in ultrahigh vacuum (UHV), ($< 10^{-9}$ torr during deposition) on a thick Au(111) buffer layer deposited on float glass platelets. A resistance

[a] e-mail: renard@ief.u-psud.fr
[b] URA CNRS 014
[c] URA CNRS 022

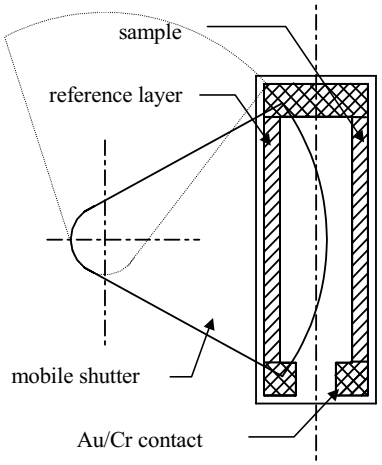


**Fig. 1.** Front view of the substrate with the two samples, the Au/Cr contacts and the mobile shutter.

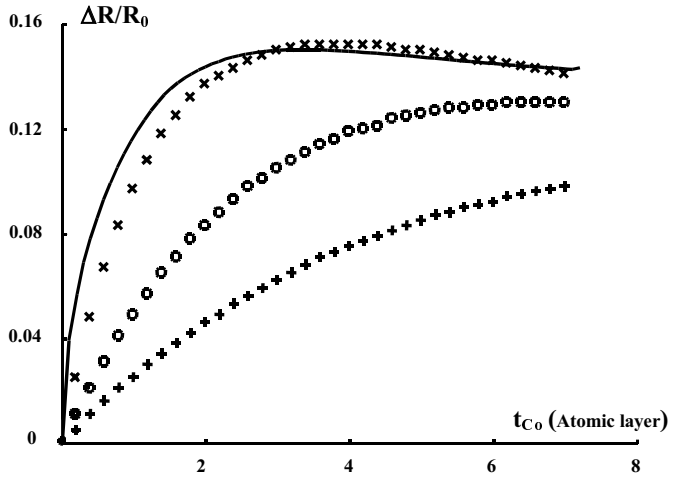


**Fig. 2.** Increase of the resistance as a function of the Co thickness ($T$ = 300 K), experimental curve obtained during deposition (—), theoretical results with $t_0$ = 0.22 nm (××), $t_0$ = 0.5 nm (○○), $t_0$ = 1 nm (++).

measurement set up, under variable magnetic field supplied by a specially designed copper coil cooled by liquid nitrogen, allowed *in situ* resistance studies. The magnetic field could be swept between −0.2 and 0.2 tesla. The temperature of the samples was accurately controlled by two copper-constantan thermocouples and could be varied between 100 and 500 K. The thickness of the deposited films was measured by a quartz micro-balance connected to a programmable frequency counter. The resistance of the sample measured by the "four-probe" technique and the evaporation speed could be followed in real time. This allowed *in situ* resistance measurements during the film growth. After the growth of a layer, the resistance could be recorded as a function of magnetic field. This measurement processes have been described in detail in a previous paper [13].

All the samples were 15 × 1.5 mm (length and width). On the float glass substrate, 20 × 10 mm, two samples could be obtained with different Co or Au thickness, by means of a mobile shutter, (Fig. 1). At first, a Au buffer layer, about 25 nm thick, was deposited at room temperature and annealed at 440 K during 60 min. The annealing process is controlled by monitoring the decrease and the stabilization of the resistance. The structure of this annealed Au buffer has been accurately determined by several different techniques including grazing X-rays reflectivity, transmission electron microscopy (TEM), reflection high energy electron diffraction (RHEED) and atomic force microscopy (AFM) [14–16]. It consists of face-centered cubic (fcc) polycrystals, of average lateral size 200 nm, with a common [111] texture. The surface exhibits atomically flat terraces (around 20 nm). An average roughness measured by AFM over 10 × 10 $\mu$m was found around 0.5 nm, this value was confirmed by X-rays measurements on the whole surface of the sample. The Co film grown on this high quality Au(111) buffer have (0001) hexagonal close-packed (hcp) structure checked on a few nm thick Co films by TEM and $^{59}$Co nuclear magnetic resonance [17]. Cross section images obtained by TEM on Co/Au multilayers show also that the Co layers become nearly continuous at Co thickness of 2-3 AL, without important degradation when piling up the different films [18].

## 3 Resistivity and magnetoresistance of Co/Au(111) single layers

### 3.1 Resistance of Co/Au(111) versus Co thickness

The resistance of Co/Au(111) was measured at room temperature *versus* the thickness of the Co layer during its growth. After a rapid increase at small thickness, $t_{Co} < 1$ AL, the resistance exhibits a broad maximum at $t_{Co} \cong 3$ AL, followed by a weak decrease at larger thickness (Fig. 2). This behavior can be qualitatively understood as following: Whereas the conduction electrons experience quasi-specular reflections on the Au buffer surfaces, the deposited Co atoms on the top surface act as scattering centers which contribute to the resistivity. In the case of epitaxial AL by AL growth, one should observe an oscillatory resistivity behavior with a period of one AL, each minimum corresponding to a complete overlayer. This behavior has been clearly evidenced in homoepitaxy of In films [19]. For Co/Au(111), the large lattice mismatch, (about 14%), forbids AL by AL growth and thus prevents resistivity oscillations. Indeed microscopic studies of the growth of Co on Au(111) single crystal show that it proceeds by nucleation of 2 AL thick Co islands, the Co layer becoming continuous around $t_{Co} \cong 3$ AL [20–22]. The resistance behavior of Figure 2 is, at least qualitatively, in agreement with this growth process. The resistance decrease observed at larger Co thickness simply reflects the Co film conductivity increase with $t_{Co}$, masked at low thickness by the rather large interface effect.

A quantitative interpretation of these resistivity data can be developed by using the Fuchs-Sondheimer model [23,24]. In this semi-classical approach, the resistivity

of Co/Au(111) film is determined by solving the Boltzmann transport equation. Bulk diffusion is characterized by two mean free paths (MFP): $\lambda_{Au}$ in gold and $\lambda_{Co}$ in cobalt. The surface effects are introduced phenomenologically by two specular parameters $p_1$ and $p_2$ which describe respectively the fraction of electrons specularly reflected at Au(111)/glass surface and at Co overlayer surface. At Co/Au interface a conduction electron can be diffused or coherently transmitted with a probability $T_{Co/Au}$.

To study the variation of the Co/Au(111) film resistance during the first stage of Co growing, it is moreover assumed that the Co layer has an island structure. According to the model of Mitchinson and Pringle [25], the proportion of the Au surface covered by Co is of the form:

$$A = 1 - \exp(-t_{Co}/t_0)$$

where $t_{Co}$ is the mean thickness of the Co layer and $t_0$ a fitting parameter called critical thickness for cobalt. We assume also that the Co islands have any sort of shape. Their lateral size is large compared to $\lambda_{Co}$ and to the film thickness. The diffusion at the islands edges gives so a negligible contribution to the film resistivity. Thus, a part $A$ of the electrons striking the film free surface is scattered by the Co islands, the other part $(1 - A)$ is scattered by the Au(111) surface. The probabilities for being transmitted to a Co island, or specularly reflected by Au surface are respectively $AT_{Co/Au}$ and $(1 - A)p_0$, where $p_0$ is the specular parameter at the Au(111) free surface.

Taking into account these boundaries conditions, we calculate the ratio $R/R_0$ of the total resistance of the film to the resistance of the Au(111) substrate as a function of $t_{Co}$ for different values of $t_0$. Numerical results are reported in Figure 2. They were obtained with the following parameters: $p_0 = 0.9$, $p_1 = 0.7$, $p_2 = 0.1$, $T_{Co/Au} = 0.8$, $\lambda_{Au} = 25$ nm and $\lambda_{Co} = 5$ nm. The initial increase of $R/R_0$ *vs.* $t_{Co}$ is larger and larger as $t_0$ decreases. The best fit with experimental data was obtained for $t_0 \cong 0.22$ nm, in good agreement with previous microscopic investigations [20–22].

Numerical results are independent of bulk scattering for thickness below 0.7 nm.

### 3.2 Temperature dependence of the resistance of Co/Au(111)

The resistance of a Co/Au(111) film with $t_{Co} = 0.6$ nm was measured as a function of the temperature in the range 100 K–300 K and compared to that of an uncovered identical Au film, made in the same deposition run. The experimental data are shown in Figure 3. It appears that the effect of the Co thin overlayer is a temperature independent contribution to the resistance. The resistivity is then given by the Matthiessen's rule:

$$\rho(T) = \rho_D + \rho_{ph}(T),$$

where $\rho_{ph}(T)$ is the temperature dependent phonon contribution and $\rho_D$ the residual resistivity as $T$ tends towards zero, including the interfacial Co/Au contribution.

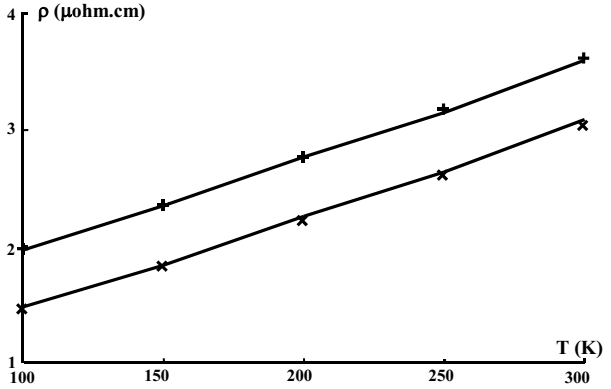


**Fig. 3.** Resistivity as a function of temperature, computed curves (—), experimental data for Au film (××), experimental data for Co/Au (++). The thickness of the Co film $t_{Co}$ is 0.6 nm.

**Table 1.**

| $T$ (Kelvin) | $\mu_0 H_c$ (Tesla) |
|---|---|
| 300 | 0.046 |
| 250 | 0.067 |
| 200 | 0.098 |
| 150 | 0.137 |
| 100 | 0.186 |

$\mu_0 = 4\pi \times 10^{-7}$ Henry/m.

These data were compared to a calculation based on the Fuchs-Sondheimer model in which the effect of the Co/Au(111) interface is simply taken into account by a strong decrease of the coefficient of specular reflectometry, $P_{Co/Au}$. The specular parameters $p_0$ and $p_1$ defined above are assumed to be temperature independent. The increase, with temperature $T$, of the resistivity $\rho$, is ascribed to a decrease of the MFP in gold $\lambda_{Au}$. By fitting the experimental data $\rho(T)$ of the Au film with theoretical curves $\rho(\lambda)$, we deduce the $\lambda_{Au}$ value for each temperature. Using these values, the Co/Au film resistivity is computed as a function of $T$, for different $P_{Co/Au}$ (Fig. 3). The best fit is found for $P_{Co/Au} = 0.08$. This value is approximately $p_2(T_{Co/Au})^2$ which corresponds to a first transmission by Co/Au interface, then a specular reflection at Co free surface and at last a second transmission by Co/Au interface.

In addition to the temperature dependence of the Co/Au(111) resistance, a resistance *versus* field hysteresis loop was recorded at a few fixed temperatures. In spite of the weakness of the MR, the coercive field, $H_c$, at which a sharp peak of resistance could be measured. The experimental values, which are the first ones, for an uncovered ultrathin film, are presented in Table 1.

### 3.3 Magnetoresistance versus thickness of the Au overlayer

The magnetoresistance of a Co layer, 0.5 nm thick, has been investigated at room temperature, for different Au

overlayer thickness. The Co layer magnetization is always perpendicular to the film plane since the critical thickness, at which the magnetization departs from perpendicular orientation is about 0.8 nm for an uncovered Co layer, and strongly increases with Au coverage. In a perpendicular applied field, a typical MR loop exhibits a resistance maximum at $+H_c$ and $-H_c$, where $H_c$ is the Co layer coercive field [13]. The magnetoresistance, defined as $\Delta R/R$ where $\Delta R$ is the height of the peak of resistance and $R$ the resistance value in zero field, is extremely small for the uncovered Co layer, ($\Delta R/R \cong 2 \times 10^{-4}$). It significantly increases with the Au overlayer thickness reaching $13 \times 10^{-4}$ for $t_{Au} = 3$ nm ($\cong$ 13 AL) (Fig. 4). The interpretation of these data is not straightforward. The MR of a single Co layer observed at $H_c$ is due to the small fraction of conduction electrons which travel from one magnetic domain to a neighboring one of opposite magnetization, without undergoing diffuse scattering between them. Thus the MR is largely determined by the size of the magnetic domains and walls and by the specular reflection coefficients, both of them depending on the Au coverage. So far, the variation of the domain size in Co/Au(111) ultrathin films has not been investigated as a function of the Au coverage. However experiments on Au/Co/Au(111) have shown a strong dependence of the domain size *versus* the Co thickness, in agreement with theory [26]. The domain size is governed by uniaxial anisotropy which varies with Co thickness. In the present case the uniaxial anisotropy varies with the Au coverage and this should lead to change the domain size. In the absence of information about the magnetic microstructure for low gold coverage, we could not perform MR calculations. The increase of MR can be interpreted also by an increase of the reflectivity of the top gold overlayer, and by the replacement of the Co/vacuum interface by the Co/Au interface, this last giving an additional spin dependent scattering. In fact a smoothing of the top surface was observed on RHEED patterns and begins as soon as is deposited a fraction of gold AL [27].

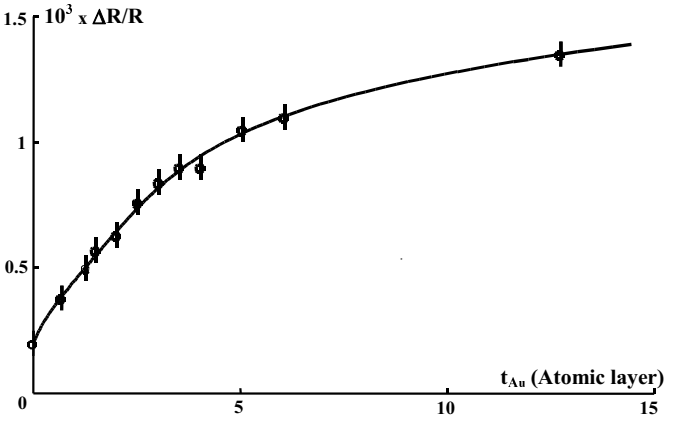


**Fig. 4.** Magnetoresistance of a simple sandwich as a function of the Au overlayer thickness, here $t_{Co} = 0.5$ nm ($T = 300$ K).

## 4 Resistivity and magnetoresistance of Co/Au(111) bilayers

### 4.1 Introduction

Thin films including two Co ferromagnetic layers separated by a thin Au spacer exhibit large magnetoresistance (GMR) related to the spin-valve effect of the two Co layers on the conduction electrons. The resistivity is larger for antiparallel configuration of the magnetizations of the Co layers than for the parallel one. Indeed, for Co, the conduction electrons of the minority band are strongly scattered, while those of the majority band are weakly scattered, $D\uparrow\downarrow \gg D\uparrow\uparrow$. In the antiparallel configuration, all the conduction electrons are strongly scattered by the Co layer with spins antiparallel to that of the majority band, whereas in the parallel configuration, the electrons with spins parallel are weakly scattered by both Co layers, and they form a low resistivity channel. This has been evidenced on Au/Co/Au/Co/Au sandwiches of uncoupled Co films with different thickness and coercivities [3] as well as on antiferromagnetically coupled Co films of same thickness [7]. In both cases, the antiparallel configuration is achieved in a certain field range $H_1 < H < H_2$, and the resistance *versus* field curve exhibits a typical mesa shape between $H_1$ and $H_2$.

The present *in situ* MR experiment allows new studies: one can accurately follow the variations of the coercive field of the Co top layer during its coverage by Au, even at submonolayer thickness, and study the MR as a function of the Au coverage thickness. An other interesting possibility is to follow the resistance during the growth of the second Co film, and to directly compare the cases of parallel and antiparallel configurations for two Au spacer thickness, yielding to respectively ferromagnetic and antiferromagnetic coupling.

### 4.2 Coercive field of a thin Co layer versus Au overlayer thickness

We performed systematic measurements of the resistance hysteresis loops at room temperature of a $Au_3$ ($t_{Au}$) / $Co_2$ (1.4 nm) / $Au_2$ (2.3 nm) / $Co_1$ (0.66 nm) / $Au_1$ (23.8 nm) as a function of the Au(111) overlayer thickness, $t_{Au}$. A few resistance *versus* field curves are shown in Figure 5. They exhibit the typical "mesa" shape between the coercive fields $\pm H_{c1}$ and $\pm H_{c2}$ of the two Co layers. One of these fields, $H_{c1}$, related to the first $Co_1$ layer is nearly independent on $t_{Au}$ whereas the second one, $H_{c2}$, is strongly dependent on $t_{Au}$ as shown in Figure 6. The $H_{c2}$ ($t_{Au}$) curve exhibits a spectacular increase at submonolayer Au coverage and a sharp maximum at $t_{Au} \cong 1$ AL, followed by a smooth minimum around $t_{Au} \cong 3$–4 AL and reaches a constant value above 5 AL. For the second $Co_2$ layer, the thickness of 1.4 nm is enough to yield an in-plane magnetization when uncovered, so that no coercive field $H_{c2}$ is observed on the curve of Figure 5a.

This dependence of the coercive field on $t_{Au}$ shows a striking similarity with the peculiar variation of the Au/Co interface anisotropy theoretically studied for an ideal Co atomic monolayer in contact with $n$ AL

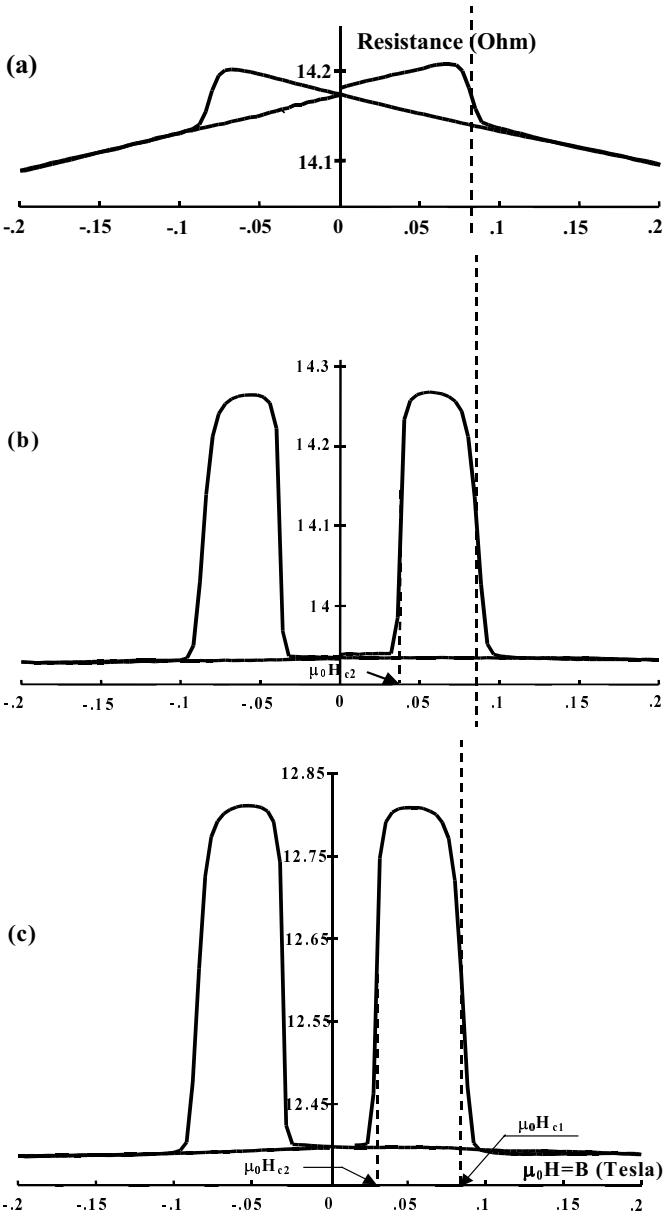


**Fig. 5.** Hysteresis loops obtained on a Co bilayer for three Au coverages. For all the bilayers, we call $Co_1$ the first Co film deposited on the gold substrate, and $Co_2$ the second Co film deposited on a gold intercalar film called $Au_2$. Here $t_{Co_1} = 0.66$ nm, $t_{Co_2} = 1.45$ nm, $t_{Au_2} = 1.4$ nm. The Au coverages thickness $t_{Au}$ are (a) $t_{Au} = 0$ AL ($Co_2$ is uncovered), (b) $t_{Au} = 1$ AL, (c) $t_{Au} = 20$ AL ($T = 300$ K in all cases).

of Au [12]. This is not completely unexpected since in all model calculations of coercive field, this later one is found to be proportional to a power of the anisotropy constant (see for instance [28] for hysteresis of Co ultrathin films). Some experiments on Co films covered by 3 or 5 nm of gold gives an identical result [29]. A maximum of anisotropy is predicted for $t_{Au} \cong 1$ AL. The maximum in coercive field here observed at 1 AL Au coverage indicates that the Au overlayer is continuous at this thickness and that the surface is nearly fully covered. Previous PMOKE anisotropy and coercive field studies of the same system have revealed

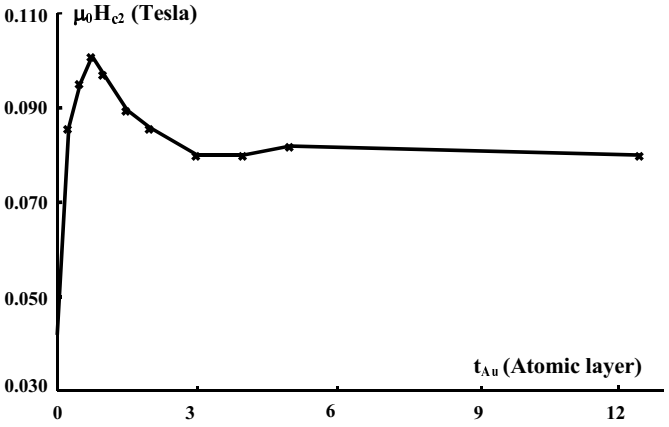


**Fig. 6.** Coercive field of the second Co film deposited ($Co_2$) as a function of the Au overlayer thickness ($T = 300$ K). Here $t_{Co_1} = 1.2$ nm, $t_{Co_2} = 0.65$ nm and $t_{Au_2} = 1.4$ nm.

a similar behavior but with a smoother dependence on $t_{Au}$ and a maximum around 1.5 AL, probably due to an imperfect growth of Au on Co in this experiment [27].

### 4.3 Magnetoresistance of the Co/Au bilayer versus Au overlayer thickness

As shown in Figure 5, the deposition of an Au overlayer strongly enhances the MR of a Co/Au bilayer. The MR is here defined as $\Delta R/R$, where $\Delta R$ is the height of the peak of resistance and $R$ the resistance value in high field. The MR, measured at room temperature, *versus* Au overlayer thickness shown in Figure 7 exhibits a rapid increase at the first Au AL coverage. Then the MR increases slowly, exhibits a broad maximum around 13 or 15 AL and slowly decreases at thickness above 20 AL. The physical origin of the quick increase with the first stages of Au growing overlayer is probably the change of a poorly specular Co surface into a highly specular Au surface as seen by RHEED [27] and also in our resistance measurements during Au deposition. Previous X-rays *in situ* experiments performed on the Co/Au system showed that the roughness of the free gold surface increases significantly for thickness larger than 3 nm [16]. This likely leads to a decrease of the reflectivity of the top Au surface which could explain the observed MR decrease after deposition of 20 Au AL.

Beyond this qualitative interpretation, we analysed our results by applying the Camley-Barnas model [30] to our $Au_3/Co_2/Au_2/Co_1/Au(111)$ layered structure. This approach is an extension of Fuchs-Sondheimer theory with spin dependent bulk and interface scattering. Bulk diffusion in Au layers is described by the same MFP, $\lambda_{Au}$, while bulk diffusion in ferromagnetic layers is characterized by two different MFP, $\lambda_{Co}\uparrow$ and $\lambda_{Co}\downarrow$ respectively for the majority (spin$\uparrow$) and minority (spin$\downarrow$) electrons. We always assume that no specular reflection occurs at Au/Co interface, thus interface diffusion is included in spin dependent transmission coefficients which also characterize

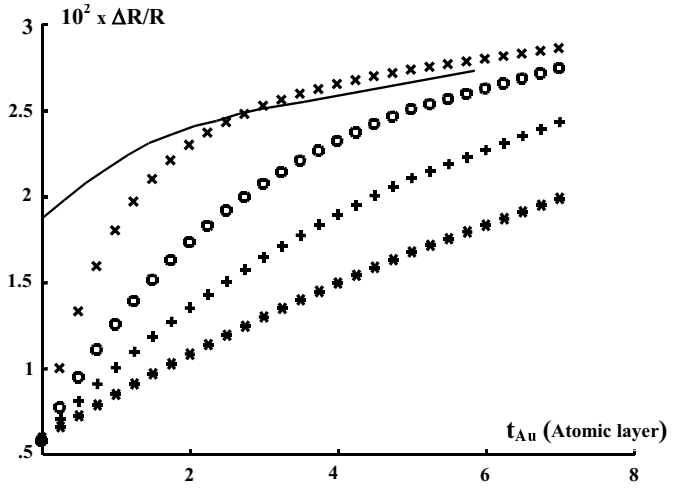


**Fig. 7.** Magnetoresistance of a bilayer as a function of the Au overlayer thickness ($T = 300$ K), $t_{Co_1} = 1.45$ nm, $t_{Co_2} = 0.7$ nm. Experimental curve obtained during deposition (—), theoretical results with $t_0^{'} = 0.2$ nm (××), $t_0^{'} = 0.5$ nm (○○), $t_0^{'} = 1$ nm (++), $t_0^{'} = 2$ nm (∗∗).

the interface quality. For the interface between $Co_i$ and $Au_j$ layers, the proportion of coherently transmitted electrons is $T_{ij\uparrow\uparrow}$ (or $T_{ij\uparrow\downarrow}$) when the electron spin is parallel (or antiparallel) to $Co_i$'s spin. The spin asymmetry of scattering defined by:

$$\alpha = (1 - T\uparrow\downarrow)/(1 - T\uparrow\uparrow)$$

is assumed to be the same for all the interfaces. The specular parameters $p_1$ and $p_3$ at the lower and upper Au surfaces are considered as spin independent. The specular parameter at the $Au_3$ free surface, $p_3$ is lower than $p_0$ because $Au_3$ is not annealed.

With these hypothesis, the resistivity of the Co/Au bilayer is computed for ferromagnetic ($\rho\uparrow\uparrow$) and antiferromagnetic ($\rho\uparrow\downarrow$) configurations. The MR defined above as $\Delta R/R$ is here:

$$(\rho\uparrow\downarrow - \rho\uparrow\uparrow)/\rho\uparrow\uparrow\,.$$

To calculate the MR of Co/Au bilayer with ultrathin Au overlayer, it is additionally assumed that $Au_3$ has an island structure, similar to that of Co layer deposited on Au substrate. With the same hypothesis as in Section 3.1, the proportion of $Co_2$ surface covered by gold is then:

$$A = 1 - \exp\left(-t_{Au}/t_0^{'}\right)$$

where $t_{Au}$ is the Au overlayer thickness and $t_0^{'}$ the critical thickness for gold. Thus, electrons striking the film free surface, which undergo coherent scattering are either specularly reflected at Co surface, or transmitted to an Au island. The probability of reflection is then $(1-A)p_2$. The probability of transmission is $AT_{23\uparrow\uparrow}$ or $AT_{23\uparrow\downarrow}$, according to the orientation of the conduction electrons spin.

With these boundaries conditions, the MR of Co/Au bilayer is computed as a function of $t_{Au}$ for different values of $t_0$. The input scattering parameters are $p_1 = 0.7$, $p_2 = 0.1$, $p_3 = 0.8$, $\lambda_{Au} = 25$ nm, $\alpha = 4$, $T_{11\uparrow\uparrow} = 0.92$, $T_{12\uparrow\uparrow} = 0.9$, $T_{22\uparrow\uparrow} = 0.88$, $T_{23\uparrow\uparrow} = 0.88$.

The above parameters are determined by the experimental curves of resistance as a function of thickness obtained during the depositions.

Theoretical curves and experimental points are reported in Figure 7. For $t_{Au} > 0.3$ nm, a good agreement between experience and theory is found for $t_0^{'} = 0.2$ nm, $\lambda_{Co}\uparrow = 13$ nm and $\lambda_{Co}\downarrow = 2.4$ nm. The spin asymmetry of bulk scattering in Co: $\lambda_{Co}\uparrow / \lambda_{Co}\downarrow$ is around 5, in agreement with the previous experimental data [31]. For the very weak thickness, there are many islands and one should have to take into account for the edges of islands, which increase scattering.

### 4.4 Resistance variation during the deposition of the second Co layer. Comparative study of ferro- and antiferromagnetic coupling across Au spacer layer

In this experiment, a first 1.4 nm thick Co layer is deposited on the annealed Au(111) buffer, and by means of the shutter, covered by Au with two different thickness: 1.8 nm leading to ferromagnetic coupling and 2.3 nm leading to AF coupling. Then the Co layer is magnetized and kept in zero field in a state of remnant magnetization. This later one is close to the saturation value, due to the large perpendicular anisotropy providing a rectangular hysteresis loop. On the two $Au_2$ (1.8 nm) / $Co_1$ (1.4 nm) / Au(111) and $Au_2$ (2.3 nm) / $Co_1$ (1.4 nm) / Au(111) samples, a $Co_2$ overlayer was deposited and the resistance was measured during the deposition as a function of the $Co_2$ thickness, $t_{Co}$. The experimental data (Fig. 8) show significantly different behaviors of $R(t_{Co})$ for the two samples. At first, for $t_{Co} < 1.5$ AL, the two samples show a similar increase of $R(t_{Co})$ related to the decrease in surface specularity due to the non magnetic Co adatoms or superparamagnetic Co islands. Between 1.5 and 2 Co AL, a step-like singularity, decrease for the sample 1 with 1.8 nm Au spacer and increase for the sample 2 with 2.3 nm Au spacer, is observed. This singularity in $R(t_{Co})$ likely happens, for the sample 1 at the thickness where the Co overlayer becomes nearly continuous and ferromagnetic at room temperature. For the sample 2 with spacer thickness 2.3 nm corresponding to antiferromagnetic coupling, an antiparallel configuration of the Co layer magnetization is established, leading to a high resistance state. Whereas for sample 1 with ferromagnetic interlayer coupling, the parallel configuration leads to a low resistance state. At further increase of $t_{Co}$, the Co overlayer magnetization turns from perpendicular to parallel to the film plane, around $t_{Co} \cong 5$ AL, leading to a second singularity in $R(t_{Co})$. In the case of antiparallel coupling, a negative step is clearly observed as shown in Figure 9.

This experimental $R(t_{Co})$ dependence could be modelized. Here we suppose that the $Co_2$ overlayer film is non magnetic at low thickness, and ferromagnetic at higher thickness with, at first, magnetization parallel (sample 1) and antiparallel (sample 2), to that of the inner film, and at large thickness nearly in-plane (Fig. 9, third part).

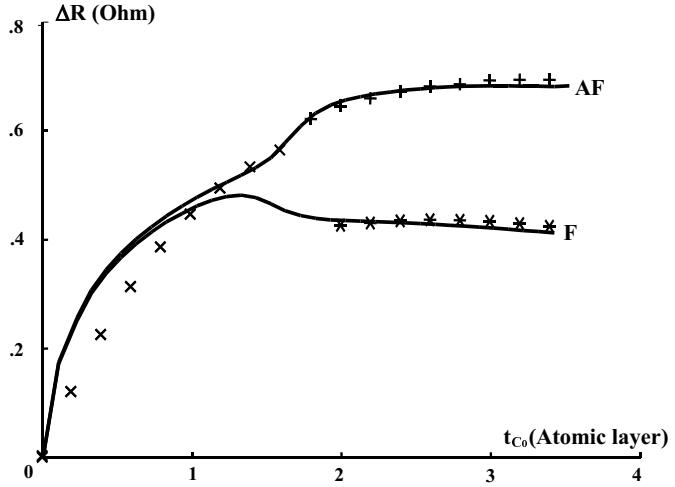


**Fig. 8.** Resistance variation as a function of the second $Co_2$ thickness, $t_{Co_1} = 1.45$ nm, ($T = 300$ K). Continuous lines are the experimental data obtained during deposition in two cases: antiferromagnetic coupling (curve AF with $t_{Au_2} = 2.3$ nm) and ferromagnetic coupling (curve F with $t_{Au_2} = 1.8$ nm). Computed values for second Co non magnetic (××), antiparallel to the first one (++), parallel to the first one (∗∗).

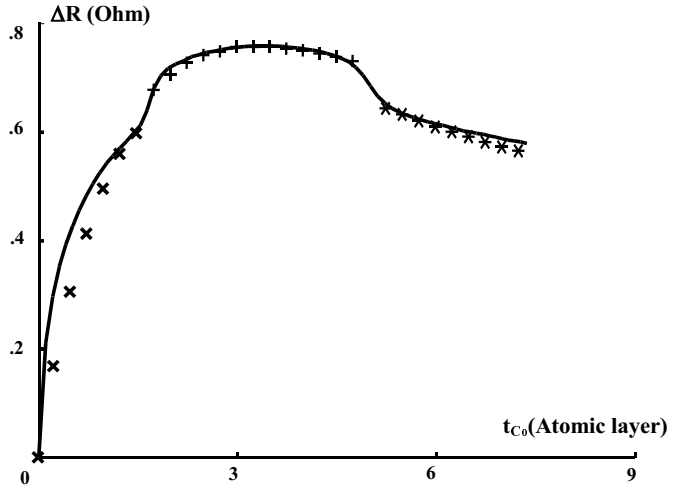


**Fig. 9.** Resistance variation as a function of the second $Co_2$ thickness in the case of AF coupling, $t_{Co_1} = 0.66$ nm and $t_{Au_2} = 2.3$ nm, ($T = 300$ K): continuous line for experimental data. Theoretical values for second Co non magnetic (××), antiparallel to the first one (++), second Co with magnetization in the plane film (∗∗).

Resistivity calculations are performed in the same way as in precedent paragraph. However, during the growing of cobalt, changes occur in the structure and in the magnetic state of the $Co_2$ layer. Thus, additional hypotheses are needed to describe the scattering at $Co_2/Au_2$ interface.

For thinner thickness, the non magnetic Co layer is composed of islands. Each island is a magnetic domain. Since the magnetization is preferentially perpendicular to the film plane, this domain structure can be assimilated, at macroscopic scale, to two domains with antiparallel moments, covering the same fraction of the $Au_2$ surface:

$$A\uparrow = A\downarrow = A/2 = 1/2\big(1 - \exp(-t_{Co}/t_0)\big).$$

Consequently, electrons striking the $Co_2/Au_2$ interface, have a probability $A/2$ to be scattered by a domain with spin parallel or antiparallel to their own spin. The transmission coefficients are the same for majority and minority electrons:

$$T_{22\uparrow} = T_{22\downarrow} = A/2\,(T_{2\uparrow\uparrow} + T_{2\uparrow\downarrow})\,.$$

This thickness range corresponds to the first part of curves in Figures 8 and 9. For the second thickness range (parts 2 in Figs. 8 and 9), the domains coalesce leading to ferro- (sample 1) or antiferromagnetic (sample 2) configuration. Nevertheless, the $Au_2$ surface is not still completely covered. Scattering at $Co_2/Au_2$ interface is described in the same way as Co1/Au1 interface (Sect. 3.1) but with spin dependent transmission.

In the case of higher thickness (third part of Fig. 9), the $Co_2$ overlayer is continuous, and its magnetization is rather in the film plane. We call $\theta$ the angle between the magnetization of the two Co layers. The transmission coefficients at $Co_2/Au_2$ interface are empirically given by [32]:

$$T_{22}\uparrow = (\cos^2\theta/2)T_2\uparrow\uparrow + (\sin^2\theta/2)T_2\uparrow\downarrow$$
for majority electrons
$$T_{22}\downarrow = (\sin^2\theta/2)T_2\uparrow\uparrow + (\cos^2\theta/2)T_2\uparrow\downarrow$$
for minority electrons.

Taking account these assumptions, we compute the resistance of this bilayer for three $Co_2$ magnetic states:

$0$ nm $< t_{Co} < 0.3$ nm, $M_2 = 0$
$0.3$ nm $< t_{Co} < 1$ nm, $M_2$ parallel or antiparallel to $M_1$
$1$ nm $< t_{Co} < 1.7$ nm, $M_2$ nearly in the film plane.

$M_1$ and $M_2$ are respectively the magnetizations of $Co_1$ and $Co_2$ layers. The calculations are performed with the parameters used for the MR studies (Sect. 4.3). Numerical results reported in Figures 8 and 9 are in good agreement with experimental data. For the third part of Figure 9, the best fit was obtained with $\theta = 90°$ corresponding to $Co_2$ magnetization lying in the film plane.

### 4.5 Loops of magnetoresistance for layers with strong antiferromagnetic coupling

The results here discussed were obtained on a $Au_3$(3.3 nm)/$Co_2$(0.4 nm)/$Au_2$(1.4 nm)/$Co_1$(1.6 nm) /$Au_1$(24 nm) sample. The thickness of the Au spacer was chosen to get an antiferromagnetic coupling as seen previously [7], and the thickness of the two cobalt layers were chosen to insure rather different coercive fields. However these thickness remain in the range of perpendicular magnetization. In this sample, the antiferromagnetic exchange field, $H_{ex}$, is higher than the coercive field of the thin layer $H_c$, so that the magnetizations of the two Co layers are antiparallel in zero applied field.

Two different hysteresis loops are shown in Figure 10. The complete hysteresis symmetrical loop of Figure 10a

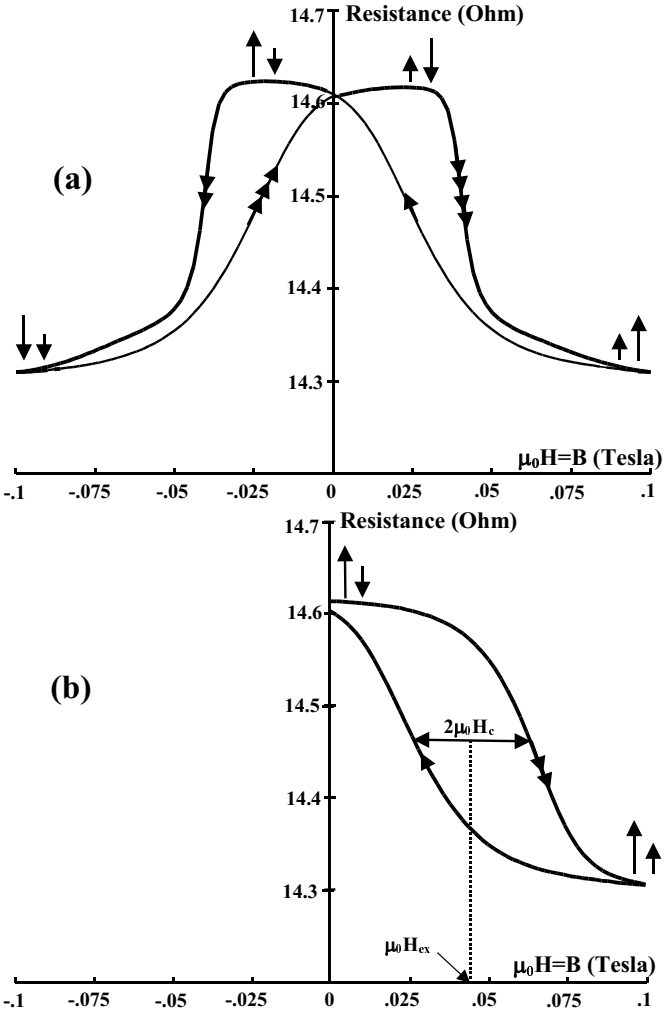


**Fig. 10.** Hysteresis loops obtained on a bilayer with a strong antiferromagnetic coupling, $t_{\mathrm{Co}_1} = 1.58$ nm, $t_{\mathrm{Au}_2} = 1.35$ nm and $t_{\mathrm{Co}_2} = 0.44$ nm, ($T = 300$ K) (a) complete symmetrical loop: small ↑ (great ↑) arrows represent respectively the magnetization of thinner (thicker) Co films. (b) small hysteresis loop.

was obtained by starting from a positive applied field $B_0 = 0.1$ tesla, leading to parallel alignment of the two Co layers magnetizations. Then the applied field was reduced to zero, reversed to $-0.1$ tesla, and returned to its initial value $B_0$. In the first step, $B = B_0 \rightarrow B = 0$, the magnetization of the thin Co layer is progressively reversed by effect of the AF exchange interaction. In the second step, $B = 0 \rightarrow B = -B_0$, the abrupt reversal of the magnetization of the thick Co layer is observed. The small hysteresis loop of Figure 10b was obtained with the same initial applied field, $B_0 = 0.1$ tesla, but after the same first step, $B = B_0 \rightarrow B = 0$, the field was increased again to $B_0$. In this experiment, the magnetization of the thick Co layer remains in the same direction, parallel to $B_0$, whereas the magnetization of the thin layer, reversed in the first step, recovers its initial direction during the second step $B = 0 \rightarrow B = B_0$. Thus Figure 10b simply shows the hysteresis loop of the thin Co layer with coercive field $H_{\mathrm{c}}$, shifted by the AF exchange field, $H_{\mathrm{ex}}$. The values obtained from the experimental data of Figure 10b are:

$$\mu_0 H_{\mathrm{c}} = 0.02 \text{ tesla} \quad \text{and} \quad \mu_0 H_{\mathrm{ex}} = 0.043 \text{ tesla}.$$

We can also remark that the reversal of the thick cobalt is mainly abrupt, but it presents a small tail, probably due to a thicker fraction of the layer with in-plane magnetization.

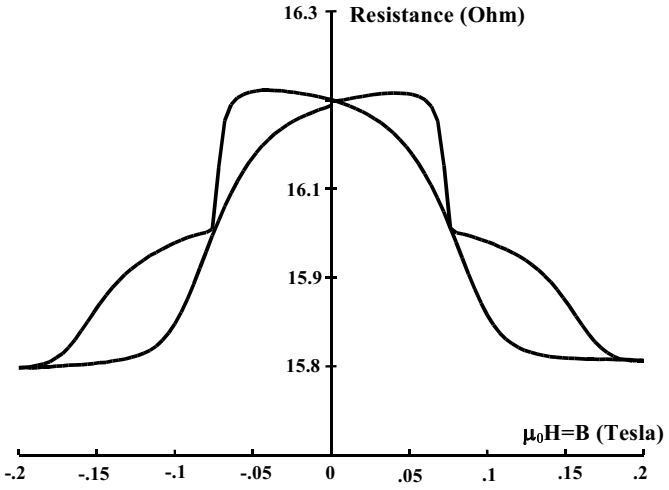


**Fig. 11.** Hysteresis loop obtained on a bilayer with strong antiferromagnetic coupling in the case of a second Co film with weak perpendicular anisotropy, $t_{\mathrm{Co}_1} = 1.2$ nm, $t_{\mathrm{Au}_2} = 1.2$ nm and $t_{\mathrm{Co}_2} = 0.6$ nm, ($T = 300$ K).

### 4.6 Loops of magnetoresistance for Co films with a weak perpendicular anisotropy

In the case of two Co films strongly coupled by AF interaction and with weak perpendicular anisotropy, *i.e.* uncovered Co with thickness close to $t^*$, a peculiar MR hysteresis loop was observed (Fig. 11). The magnetizations which are antiparallel in zero field, become at a well defined field in a configuration with an angle $\theta \neq (0, 180°)$, and become progressively parallel at higher field. For $\theta$ around 90°, the MR value is 1/2 of the MR maximum value. This phenomenon can be interpreted as a spin-flop transition, which is usual for weakly anisotropic antiferromagnets. The spin-flop transition takes place between the AF configuration with the magnetization of a film along the field and that of the other one antiparallel to the field, and a configuration at which the magnetizations are oblique with respect to the field. We did not perform the calculations in the experimental situation of Figure 11, because the anisotropy constants of the uncovered thin film are not accurately known. These calculations should take into account both anisotropy contributions of order 2 and 4, this latter contributions favoring the oblique configurations. Furthermore, a biquadratic coupling between the films cannot be excluded. It also favors an oblique configuration with $\theta$ around 90°.

## 5 Conclusion

Detailed investigations on resistance and magnetoresistance (MR) of Co/Au(111) sandwiches and bilayers with perpendicular magnetization were performed. For the first time, to our knowledge, the experiments were carried out *in situ*, in ultrahigh vacuum during the films deposition. This allowed reliable data about the Co/Au interface formation and the thickness dependence of MR.

On single sandwiches, we obtained a large increase of the film resistance in the first stages of the growth of the Co layer. From Co thickness about one atomic layer, calculations based on a phenomenological model are in good agreement with experimental data. Temperature dependence of the resistance of Co/Au(111) was also investigated and allowed determination of parameters which characterize, for electrons of conduction, the interface between Co and Au. Coercive field of uncovered Co film was measured for different temperatures.

Hysteresis loops of Co/Au bilayers were studied as a function of Au overlayer thickness. In first, we observed a variation of the coercive field of the second Co layer which reflects theoretical predictions about Au/Co interface anisotropy. Increase of MR as a function of Au coverage thickness was obtained experimentally. It was interpreted using the Camley-Barnas model with spin-dependent bulk and interface scattering. Next we studied coupling across the Au spacer layer, during the growth of Co top layer, and compared to calculations. Finally, hysteresis loops of strongly antiferromagnetically coupled bilayers were presented and explained qualitatively.

Our experimental results are in good agreement with theoretical calculations, except for Au (or Co) coverages lower than one AL. This discrepancy is probably due to an additional scattering at the edges of islands which constitute the layers at very low thickness. This contribution is difficult to evaluate, without information on the shape, the number and the size of the islands. *In situ* AFM or STM studies during the growth of the films are expected in a next future, to precise this point.

## References


1. C. Chappert, K. Le Dang, P. Beauvillain, H. Hurdequin, D. Renard, Phys. Rev. B **34**, 3192 (1986).
2. J.P. Renard, P. Beauvillain, Phys. Scr. **T49**, 405 (1987); E. Vélu, C. Dupas, D. Renard, J.P. Renard, J. Seiden, Phys. Rev. B **37**, 668 (1988).
3. C. Dupas, P. Beauvillain, C. Chappert, J.P. Renard, F. Trigui, P. Veillet, E. Vélu, D. Renard, J. Appl. Phys. **67**, 5680 (1990).
4. F. Trigui, E. Vélu, C. Dupas, J. Magn. Magn. Mater. **93**, 421 (1991).
5. M.N. Baibich, J.M. Broto, A. Fert, F. Nguyen Van Dau, F. Petroff, P. Etienne, G. Creuzet, A. Friederich, J. Chazelas, Phys. Rev. Lett. **61**, 2472 (1988).
6. G. Binasch, P. Grünberg, F. Saurenbach, W. Zinn, Phys. Rev. B **39**, 4828 (1988).
7. V. Grolier, D. Renard, B. Bartenlian, P. Beauvillain, C. Chappert, C. Dupas, J. Ferré, M. Galtier, E. Kolb, M. Mulloy, J.P. Renard, P. Veillet, Phys. Rev. Lett. **71**, 3023 (1993).
8. P. Bruno, C. Chappert, Phys. Rev. Lett. **67**, 1602 (1991); Phys. Rev. B **46**, 261 (1992).
9. F.J.A den Broeder, D. Kuiper, A.P. van de Mosselaer, W. Hoving, Phys. Rev. Lett. **60**, 2769 (1988).
10. B.N. Engel, M.H. Wiedmann, C.M. Falco, J. Appl. Phys. **75**, 6401 (1994) and references there in.
11. P. Beauvillain, A. Bounouh, C. Chappert, R. Mégy, S. Ould-Mahfoud, J.P. Renard, P. Veillet, D. Weller, J. Corno, J. Appl. Phys. **76**, 6078 (1994).
12. B. Ùjfalussy, L. Szunyogh, P. Bruno, P. Weinberger, Phys. Rev. Lett. **77**, 1805 (1996).
13. J. Corno, M. Galtier, D. Renard, J. Magn. Magn. Mater. **174**, L10-L16 (1997).
14. L. Nevot, B. Pardo, J. Corno, Phys. Rev. Appl. **23**, 1675 (1988).
15. D. Renard, G. Nihoul, Phil. Mag. B **55**, 7 (1987).
16. C. Marlière, D. Renard, J.P. Chauvineau, Thin Solid Films **201**, 317 (1991).
17. C. Cesari, J.P. Faure, G. Nihoul, K. Le Dang, P. Veillet, D. Renard, J. Magn. Magn. Mater **78**, 296 (1989).
18. N. Mliki, Ph.D. thesis, University of Toulon, France, 1993.
19. J.P. Chauvineau, C. Pariset, Surf. Sci. **36**, 155 (1973).
20. B. Voigtländer, G. Meyer, N.M Amer, Phys. Rev. B **44**, 10354 (1991).
21. C. Tölkes, P. Zeppenfeld, M.A. Krzyzowski, R. David, G. Comsa, Phys. Rev. B **55**, 13922 (1997).
22. N. Marsot, R. Belkou, F. Scheurer, B. Bartenlian, N. Barrett, C. Guillot, Surf. Sci. **377-379**, 225 (1997).
23. K. Fuchs, Proc. Camb. Philos. Soc. **34**, 100 (1938).
24. E.H. Sondheimer, Adv. Phys. **1**, 1 (1952).
25. J.C. Mitchinson, R.D. Pringle, Thin Solid Films **7**, 427 (1971).
26. M. Speckmann, H.P. Oepen, H. Ibach, Phys. Rev. Lett. **75**, 2035 (1995).
27. S. Ould-Mahfoud, R. Mégy, N. Bardou, B. Bartenlian, P. Beauvillain, C. Chappert, J. Corno, B. Lecuyer, G. Sczigel, P. Veillet, D. Weller, M.R.S. Proc. Spring Meeting **313**, 251 (1993).
28. P. Bruno, G. Bayreuther, P. Beauvillain, C. Chappert, G. Lugert, D. Renard, J.P. Renard, J.P. Seyden, J. Appl. Phys. **68**, 5759 (1990).
29. A. Kirilyuk, J. Ferré, V. Grolier, J.P. Jamet, D. Renard, J. Magn. Magn. Mater. **171**, 45, (1997).
30. J. Barnas, A. Fuss, R.E. Camley, P. Grünberg, W. Zinn, Phys. Rev. B **42**, 8110 (1990).
31. B.A. Gurney, V.S. Speriosu, J.P. Nozières, H. Lefakis, D.R. Wilhoit, O.U. Need, Phys. Rev. Lett. **71**, 4023 (1993).
32. R.E. Camley, J. Barnas, Phys. Rev. Lett. **63**, 664 (1989).